Recent development of the triboelectric properties of the polymer: A review

Hanjun Ryu[1], Sang-Woo Kim[1,2*]

[1]*School of Advanced Materials Science and Engineering, Sungkyunkwan University (SKKU), 2066 Seobu-ro, Suwon, 16419, Republic of Korea*
[2]*SKKU Advanced Institute of Nanotechnology (SAINT), Sungkyunkwan University (SKKU), 2066 Seobu-ro, Suwon, 16419, Republic of Korea*

*Corresponding author

DOI: 10.5185/amlett.2018.1869
www.vbripress.com/aml

Abstract

Smart sensors and network systems are commonly referred to as Internet of Things (IoT) and are being used to realize a smart society. Although the development of low-power smart systems and large-capacity batteries is increasing the usage time of IoT devices, the time-limited capability of such systems reveals a need for self-powered sensors and systems for sustained IoT use. Mechanical energy is easily accessible from the environment to power sensors and systems. The triboelectric nanogenerator (TENG) converts mechanical energy into electric energy was first introduced in January 2012 by Wang *et al*., and we describe recent developments in the triboelectric properties of the polymers because the contact electrification between the two different materials is a key factor of TENG. This review article discusses the four operating modes of TENG, the working mechanism, the theoretical modelling of the vertical TENG, and the research aspects of the material. Copyright © 2018 VBRI Press.

Keywords: Triboelectric, nanogenerator, energy harvesting, energy conversion, polymer.

Introduction

Recently, smart sensors and network systems, which are also referred to as IoTs, are being used to realize a smart networking society [**1-3**]. These IoTs are being used in applications useful for daily life [**4, 5**]. However, it is difficult to connect electric wires directly to multitudinous sensors and a battery needs to be used as a temporary power source [**6, 7**]. Due to limited power capacity and operating time, extending the operating time is a critical issue [**8**]. A typical approach is to enlarge the capacity of battery, and another approach is to develop highly power efficient sensors and networking systems to extend the operating time [**9**]. However, without additional energy charge during system operation, ultra-low power consumption systems and large capacity batteries cannot ensure permanent operation. Therefore, there is a demand for self-powered sensors and systems to overcome such time-limited systems [**10**].

Generally, there are a variety of accessible green energy sources that are converted into electrical energy [**11-16**]. Photovoltaic [**17, 18**], thermoelectric [**19, 20**], pyroelectric [**21, 22**], piezoelectric [**23, 24**] and triboelectric [**25, 26**] energy converting systems have been investigated to realize self-powered electronics. Mechanical energy is one of the most widespread and abundant energy sources and it is a promising energy source for powering small electronics [**27**]. Thus, among energy conversion systems, triboelectric energy converting systems have recently become more promising because TENG utilizes mechanical energy as an input energy source and adapts to various mechanical energy types in a variety of operating modes, such as vertical contact and separation mode [**28**], lateral sliding mode [**29**], single electrode mode [**30**] and freestanding triboelectric layer mode [**31**]. Therefore, the combination of a sensor and TENG is going to allow the sensor to operate and harvest energy at the same time [**32**]. In practice, smart sensors and network systems have a certain sampling rate and periodically consume energy [**33**]. In other words, an IoT system operates in sleep and active modes while the sleep mode has a much longer in duration than active mode with minimal power consumption [**34**]. In addition, since TENG constantly harvests energy and charges the battery, the energy collected during the sensor's sleep mode cycle to provide sufficient power to activate smart sensors and network systems. **Fig. 1.**

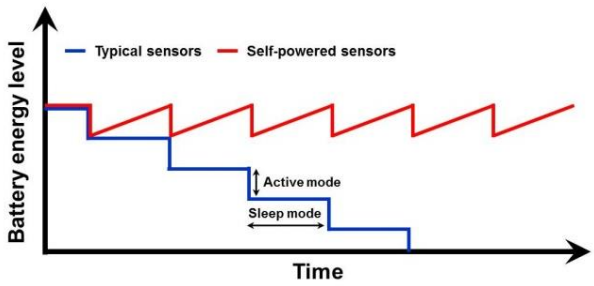

Fig. 1. Schematic description of the battery energy level during the sleep and activate mode of typical sensors and self-powered sensors (inspired from Ref. [**33**]).

schematically describes the battery lifetime of both typical sensors and self-powered sensors. Typical sensors normally consume energy in the active mode and conserve energy in the sleep mode [**35**]. Even if the power consumption of the sensor decreases or the battery capacity increases, battery replacements are still required [**36**]. On the other hand, self-powered sensors using TENG can charge the battery during sleep to realize permanent smart sensors [**37**]. Therefore, implementing self-powered sensors requires high-performance TENG, battery and power management circuits [**38, 39**]. In particular, TENG is the most important part for self-powered sensors, so we describe recent developments in the triboelectric properties of the polymers for high power performance TENG.

Triboelectric nanogenerators

TENGs convert mechanical energy into electric energy based on triboelectrification and electrostatic induction [**40, 41**]. When two different materials come into contact with each other, both materials have surface charges with opposite polarity, which are known as triboelectric charges (See **Fig. 2a.**) [**42**]. Triboelectric series determine the polarity of the surface triboelectric charges, and these charges are the main source of electrostatic induction in electrodes with certain potential differences [**43**]. After the formation of surface triboelectric charges, the relative positional change in the two materials through external mechanical energy induces an electric potential difference between the electrodes and causes the electric charge to flow through the external circuit to maintain the electrostatic equilibrium (See **Fig. 2b-2d.**) [**44**]. Therefore, mechanical energy is converted into electricity using this well-known mechanism.

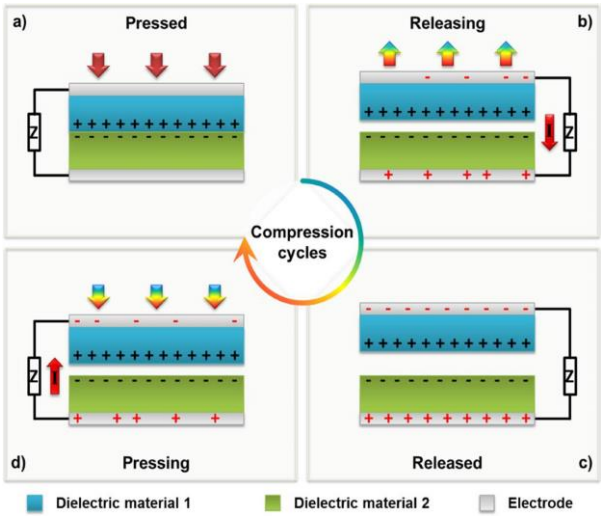

Fig. 2. Vertical contact mode working mechanism for TENG. (a) Triboelectrification process at the interface between two dielectric materials by external force. (b) The electrostatic induction process through external circuit to balance the potential during release. (c) Fully balanced potential difference state by an external force. (d) Electrostatic induction process through an external circuit to balance the potential during pressing. Adapted from Ref. [**53**] with permission from Wiley.

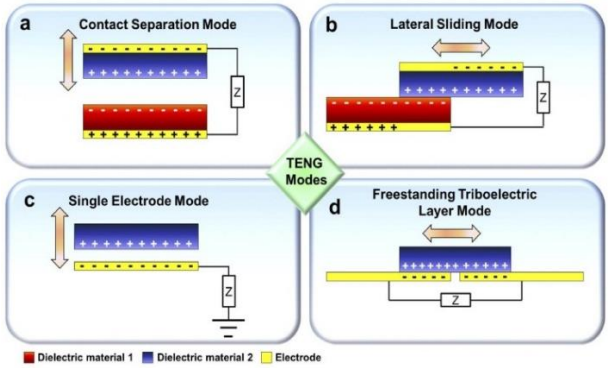

Fig. 3. Schematic description of four TENGs (a) Vertical contact and separation mode TENG. (b) Lateral sliding mode TENG. (c) Single electrode mode TENG. (d) Freestanding triboelectric layer mode TENG. Adapted from Ref. [**34**] with permission from AIP Publishing.

As described above, TENGs can utilize various mechanical energy types, including vertical motion [**45**], lateral motion [**46**] and rotational motion [**47**]. As described in **Fig. 3.**, the four TENG modes consist of different configurations of the triboelectric layer and electrode [**48**]. Thus, the triboelectric layer will be carefully determined according to the type of mechanical energy to ensure stable electron transfer capability [**49**]. The surface morphology, compressive strain stability and electron transfer capability are important to maintain a stable performance in contact separation mode and single electrode mode TENGs [**50**]. For lateral sliding mode and freestanding triboelectric layer mode TENGs, the coefficient of friction, wear resistance and thermal resistance are crucial factors the ensure stability because they retain the surface triboelectric charges much harder than in other modes [**51**]. In other words, it is impossible to maintain high-performance TENGs without precise material design [**52, 53**].

Here, we focus on vertical contact mode TENG to analyze its material aspects. The voltage between the electrodes (V), the total transferred charge between the electrodes (Q), and the separation distance of two triboelectric layers (x) are the three core parameters of the basic theoretical equation that represents the power performance of the TENG [**54**]. Depending on the triboelectric material pair, TENG is classified as dielectric to dielectric TENG and conductor to dielectric TENG [**53**]. Both TENG models are shown in **Fig. 4.** as in Ref. [**54**].

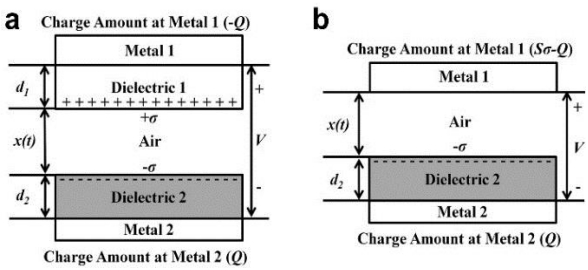

Fig. 4. (a) Theoretical structure of dielectric-to-dielectric **TENG**. (b) Theoretical structure of dielectric-to-metal TENG. Adapted from Ref. [**53**] with permission from Royal Society of Chemistry.

There are two dielectric layers, each with a thickness of d_1 and d_2, and the relative dielectric constants ε_{r1} and ε_{r2} have the same active area (S). A metal layer is deposited as an electrode beneath the two triboelectric dielectric layers. The distance between the dielectric layers can change under external mechanical forces. After contact electrification by external forces between the two dielectric layers, the interface has the opposite surface charges density (σ) with equal quantity. Since these triboelectric charges form on the dielectric layers, the surface charges are assumed to be uniformly distributed on the surfaces [**55**]. When the two dielectric layers begin to separate from the contact state with an increase in x, a potential difference (V) will be induced. The total transferred charges (Q), which are induced by the potential represent the amount of charges on the electrodes. With this model, the dielectric to dielectric contact-mode TENG V-Q-x relationship can be derived using equation (1) [**53**].

$$V = -\frac{Q}{S\varepsilon_o}\left(\frac{d_1}{\varepsilon_1} + \frac{d_2}{\varepsilon_2} + x(t)\right) + \frac{\sigma x(t)}{\varepsilon_o} \quad (1)$$

The model for the conductor to dielectric TENG has Metal 1 instead of Dielectric 1. Therefore, the total charge in metal 1 is the surface triboelectric charge ($S\cdot\sigma$) and the transferred charges between the two electrodes ($-Q$), so the total charges in Metal 1 are ($S\cdot\sigma$-Q). With this model, the conductor to dielectric contact-mode TENG V-Q-x relationship can be derived using equation (2) [**53**].

$$V = -\frac{Q}{S\varepsilon_o}\left(\frac{d_2}{\varepsilon_2} + x(t)\right) + \frac{\sigma x(t)}{\varepsilon_o} \quad (2)$$

Based on equation (1) and (2), it is able to provide important guidance for the specific design of TENG as a permanent power source.

Materials for TENG

Since the triboelectric series were reported [**56**], many research groups have investigated and synthesized new materials for the triboelectric layer [**57**]. *Zhang et al* reported a triboelectric fiber based wearable textile TENG (see **Fig. 5.**) [**58**]. In addition, the weaving textile TENG or knitting textile TENG was made using two different conductive threads to enhance output performance. Poly(amide) fibers, nylon, were one of the most positive triboelectric materials [**9**], and the cellulose fibers, cotton, which can react with chlorosilanes to form surface grafted siloxanes that are chemically functionalized by silanes and regulated as negative triboelectric materials. Thus, the nylon textile that has a positive triboelectric material, functionalized cotton (F-cotton) textile with a negative triboelectric material, and conductive textile with an electrode composed of the textile TENG. Both triboelectric textiles were sown to the conductive textiles to reduce the contact resistance and ensure efficient electrostatic induction. Due to the difference in the work function, the surface charge generated between F-cotton and nylon textiles could be maximized (see **Fig. 5a.**).

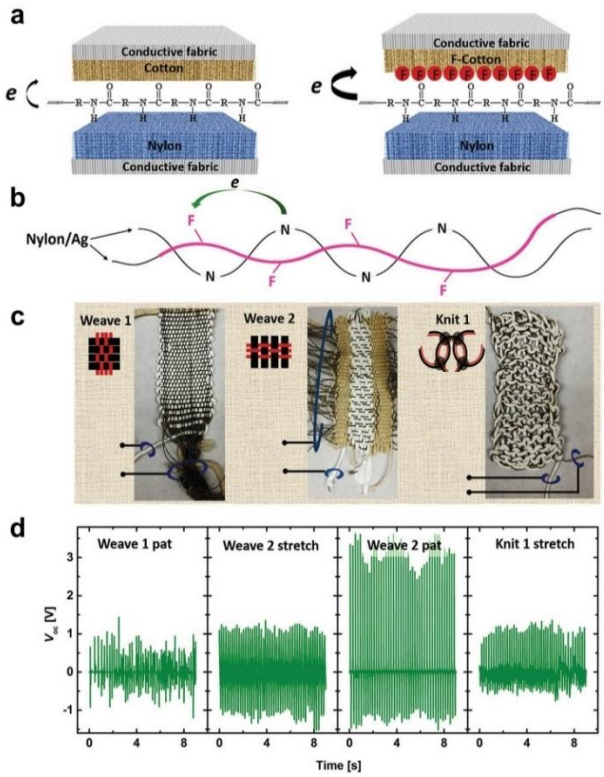

Fig.5. (a) Schematic image of textile TENGs. (b) Schematic illustration of a two-in-one triboelectric thread. (c) Optical images of textile TENGs. (d) Open circuit voltage of textile TENGs. Adapted from Ref. [**58**] with permission from Wiley.

Also *Zhang et al* reported two-in-one triboelectric textiles that were fabricated using a conductive nylon thread and polytetrafluoroethylene (PTFE) wrapped conductive nylon thread (see **Fig. 5b.**). **Fig. 5c.** showed optical images of two woven (Weave 1 and Weave 2) and one knitted triboelectric textile (Knit 1). A schematic illustration of the Weave 1, Weave 2 and Knit 1 next to the optical images demonstrated a brief pattern of triboelectric textiles. The Weave 1 TENG was generated around 1 V by gentle touching, and Weave 2 TENG generated over 1 V or 3 V via gentle stretching or patting respectively. The two different threads for Knit 1 TENG were contacted throughout the textile, and knots allowed additional contact sites for threads that were highlighted by the dots in **Fig. 5c.,** the schematic image of Knit 1. Theoretically, the porous structure of Knit 1 TENG should provide sufficient space and a large displacement between the threads, which results in large amounts of charge transfer between the electrodes. However, Knit 1 TENG generated around 1 V because Knit 1 TENG had insufficient friction points compared to the Weave TENG. Optimizing the knitting textile will increase the contact area between the positive triboelectric thread and negative triboelectric thread of the TENG and will provide additional contact sites. Therefore, a proper balance between ample spacing between the threads and the density of the contact points achieves the most efficient friction and maximum charge collection to improve the output of the textile TENG.

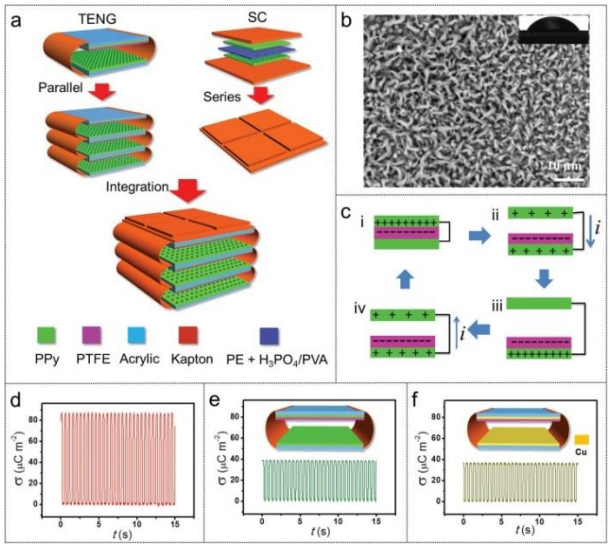

Fig. 6. (a) Schematic description of all-plastic TENG. (b) Surface scanning electron microscope (SEM) image of hPPy. (c) Working mechanism of the TENG. (d) Surface charge density of the TENG with hPPy triboelectric layer and cPPy back electrode. (e) Surface charge density of the TENG with cPPy triboelectric layer and cPPy back electrode. (f) Surface charge density of the TENG with Cu triboelectric layer and Cu back electrode. Adapted from Ref. [**59**] with permission from Wiley.

Another approach is to utilize a conductive polymer, as reported by *Wang et al* [**59**]. Conducting polypyrrole (cPPy) based TENG utilized cPPy as a triboelectric layer and electrode material instead of a metal. In particular, a novel hollow hornlike morphology (hPPy), a surface treated cPPy, was applied as a triboelectric layer. As shown in **Fig. 6.**, hPPy was used as a triboelectric layer and electrode, and the PTFE/cPPy layer was used as the counter triboelectric layer composed of a PTFE friction layer and cPPy back electrode. Three TENGs were stacked and connected in parallel to improve the output performance. The micro horns for hPPy were synthesized to be dense and homogeneous with an average 100 nm diameter, 5 ~ 10 μm length and approximate density as 10^6 ~ 10^7 per cm^2. This unique surface structure of hPPy enlarged the effective contact area and contact electrification on the surface. **Fig. 6c.** showed the working mechanism of the basic vertical contact-separation mode hPPy-based TENG, which was a coupling of the triboelectrification and electrostatic induction. As described above, the triboelectric surface charge density (σ) was an important parameter of the TENG performance, so *Wang et al* analyzed the triboelectric surface charge density of hPPy, cPPy and copper (Cu) based TENGs, respectively (see **Fig. 6d-6f.**). The charge density of cPPy-based TENG and Cu-based TENG were both about 40 μCm^{-2}. However, the hPPy-based TENG was about 84 μCm^{-2}, which was twice higher than that of the other surface charge density. In addition, the hPPy-based TENG generated two times higher power performance than that of the other triboelectric layer TENGs. They proposed two aspects to improve the surface charge density and the performance of the hPPy-based TENG.

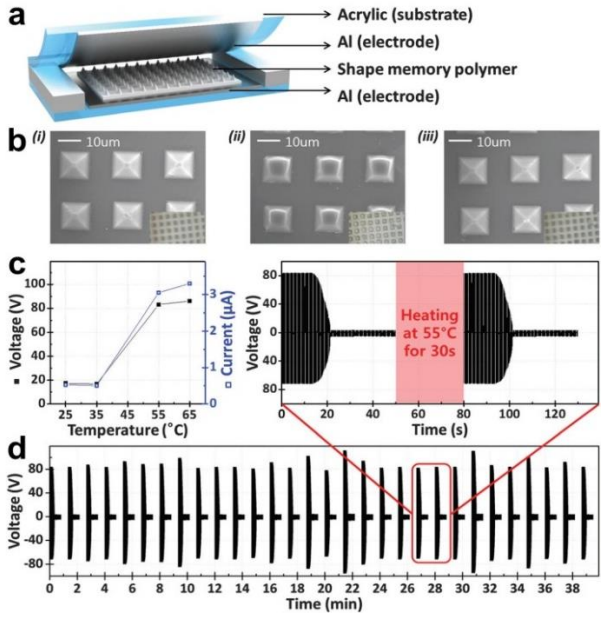

Fig. 7. (a) Schematic image of SMP-TENG. (b) Surface SEM images of the SMP; (i) initial state, (ii) after degradation by force, (iii) after the healing process. (c) Output voltage and current of SMP-TENG depending on the healing temperature. (d) Output voltage of SMP-TENG after rapid degradation and self-healing processes (30 times cycle). Adapted from Ref. [**62**] with permission from Royal Society of Chemistry.

The enlarged effective contact area due to the microstructure of the surface and shape adaptive contact behavior of surface treated hPPy led to efficient triboelectrification [**60, 61**]. Therefore, the potential of conductive polymer based TENG and surface treatment can be controlled to optimize the output performance.

Improving the reliability of TENG is important as improving the performance. A deterioration of the surface micropattern on the triboelectric layer due to external mechanical forces results in a degradation in TENG performance. As a consequence, the output voltage and current are reduced, and therefore the output power of the TENG is dramatically reduced. *Lee et al* reported the shape memory polymer (SMP) to extend the TENG lifetime and to allow a reconstruction of the micropatterns [**62**]. The vertical contact separation mode TENG was made on the surface of the micro pyramid patterned negative triboelectric shame memory polyurethane (SMPU) and aluminum (Al) electrode (see **Fig. 7.**). The SMPU pyramidal micropattern was greatly deformed by an external compressive force of 10 kgf at room temperature. This degradation in the surface micropattern dramatically reduced the SMPU-TENG performance **(Fig. 7.b.).** After the surface pattern degradation, the output voltage and current decreased from 83 V and 3 μA to 17 V and 0.5 μA respectively. To recover the surface micropattern of the SMPU-TENG, *Lee et al* raised the entire device temperature from 25°C to 65°C using a hot plate. After the temperature reached a glass transition temperature (T_g) of 55°C due to the inherent characteristics of the SMPU, the SMPU recovered its original pyramid surface micropattern. Therefore, after

SMPU-TENG healing, the output voltage and current also recovered to their original power performance. In addition, they performed 30 consecutive deterioration and healing cycles in the same SMPU-TENG to confirm the repeatability and stability of the SMPU. This demonstration showed that the SMPU-TENG could be healed after the SMPU micropattern and performances degradation, and could recover its energy harvesting capabilities. Therefore, a new smart self-healing polymer-based TENG provides an innovative way to recover TENGs from degradation due to excessive external mechanical forces.

Polymer development for high power TENGs

Over the past several decades, the development of polymer properties has been studied and many key elements that improve polymer properties have been researched [**63**]. *Kim et al* reported that the ferroelectric properties and TENG performance improved by increasing the crystallinity of the ferroelectric polymer [**64**]. The ferroelectric polymers were one of the most promising candidates for triboelectric layers because they had inherent properties that could be changed from negative to positive by a poling process. Tetrahydrofuran (THF), methylethl ketone (MEK), dimethylformamide (DMF) and demethylsulfoxide (DMSO) had dipole moments of 1.75, 2.7, 3.8, 4.1 D at 20°C, respectively, and were considered as P(VDF-TrFE), ferroelectric polymer, solvents. **Fig. 8a.** showed a schematic illustration of the P(VDF-TrFE) dissolved in a low dipole moment solvent and a high dipole moment solvent. The P(VDF-TrFE) dissolved in a high dipole moment solvent was predicted to form a longer chain length, better orientation and higher crystallinity [**65, 66**]. To investigate the relationship between the solvent and crystallinity, the P(VDF-TrFE) thin films were prepared using four different solutions, and X-ray diffraction (XRD), differential scanning calorimetry (DSC) measurements were performed. **Fig. 8b.** showed the results of the XRD measurements and confirmed the β phase of P(VDF-TrFE) [**21**]. Although the four solvents-based P(VDF-TrFE) had a β-phase, the higher crystalline P(VDF-TrFE) had a lower value of full width at half maximum (FWHM) at the β-phase peak position [**67**]. THF, MEK, DMF and DMSO had values of 0.79, 0.78, 0.74 and 0.70 FWHM, respectively, and demonstrated that the high dipole moment solvent had a higher crystalline P(VDF-TrFE). Based on the DSC measurement results, they calculated the percentage of the crystallinity ratio of P(VDF-TrFE) using equation (3) [**68**].

$$X_c = \left(\frac{\Delta H_m}{\Delta H_m^0}\right) \times 100\ \% \qquad (3)$$

X_c was the crystallinity percentage, ΔH_m was the melting enthalpy, and ΔH_m^o was the melting enthalpy of a 100 % crystalline P(VDF-TrFE) (i.e., 91.45 mJ mg^{-1} [**69**]). The extracted ΔH_m values of four P(VDF-TrFE) samples were 16.9, 21.1, 23.0 and 23.4 $mJmg^{-1}$, respectively, from the DSC heating curves. Thus, the crystallinity of P(VDF-TrFE) based on THF, MEK, DMF and DMSO solvents were 18.48 %, 23.07 %, 25.15 % and 25.59 %, respectively. In addition, the gel permeation chromatography (GPC) measurements showed that a higher dipole moment solvent formed a longer chain length and higher molecular weight. Using the developed P(VDF-TrFE) layers, the vertical contact and separation mode TENGs were fabricated (see **Fig. 8c.**). When the Al and P(VDF-TrFE) triboelectric layers contact the 1 kgf at 3 Hz, the output voltage and current for THF, MEK, DMF and DMSO-based TENG were 206 V and 126.9 μA, 234V and 147.8 μA, 251 V and 180.5 μA, and 340 V and 220 uA, respectively. Compared to a low dipole moment solvent and high dipole moment solvent, the power performance of the DMSO-based TENG significantly enhanced the voltage up to about 65 % with a current of up to 75 %. Therefore, the strategy to increase the crystallinity of the polymer provides a promising way to develop polymers for high performance TENG.

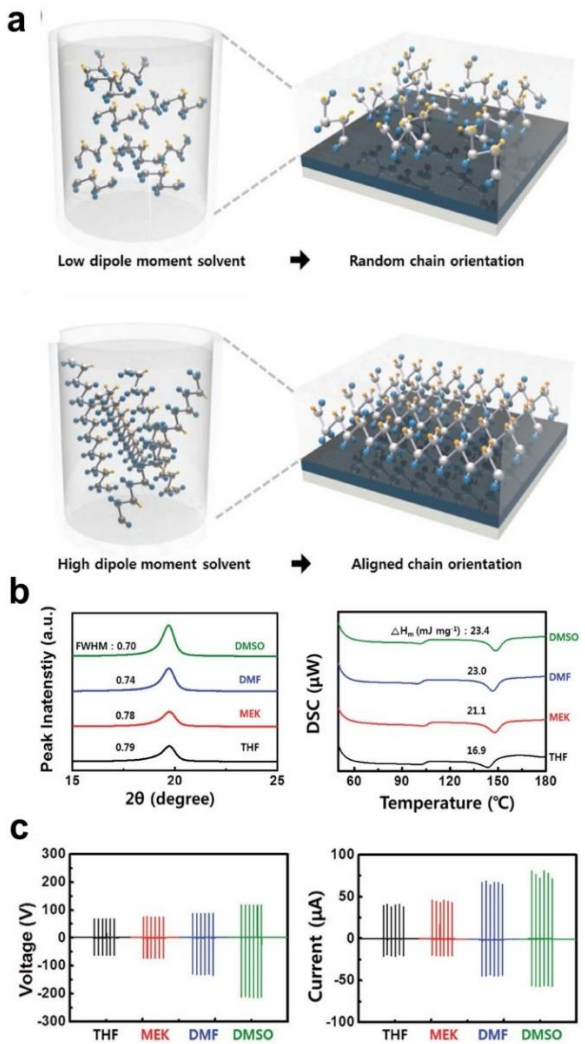

Fig. 8. (a) Schematic images of P(VDF-TrFE) dissolved in low dipole moment solvent and high dipole moment solvent. (b) XRD and DSC measurement results of the P(VDF-TrFE) dissolved in THF, MEK, DMF and DMSO solvents. Adapted from Ref. [**64**] with permission from Wiley.

Another approach is the surface functionalization that was reported by *Shin et al* [70]. They investigated the atomic level chemical functionalization effect of the polymer surface on the triboelectrification effect, and proper chemical functionalization of polymer surfaces could modify a wide range of triboelectric properties. **Fig. 9a.** described the polymer surface of the chemical functionalization with various molecules. Poly(ethylene terephthalate) (PET) was cost-effective, accessible, and solution processable. In addition, the oxygen plasma treatment on PET could easily form hydroxyl groups (-OH) on the surface [**71**], and this hydroxyl surface groups provided a strong covalent bond between the proper functionalized groups and the PET. To negatively functionalize the surfaces, halogen-terminated "aryl"-silane derivatives, triethoxy(*p*-halophenethyl) silane (p-XC_6H_4)$CH_2CH_2Si(OEt)_3$, were synthesized: triethoxy(phenethyl) silane (X = H), triethoxy (4-bromophenethyl) silane (X = Br), triethoxy (4-fluorophenethyl) silane (X = F), and triethoxy (4-chlorophenethyl)silane (X = Cl). To simplify this, they named H-PET, Br-PET, F-PET and Cl-PET, respectively (see **Fig. 9a.**). To positively functionalize the surfaces, the aminated materials were utilized, including linear polyethylenimine (PEI(l)), hexyltrimethoxysilane (HTMS), poly-L-lysine (PLL), 3-aminopropyltrimethoxysilane (APTES), and branched polyethylenimine (PEI(b)). To simplify this, they named PEI(l)-PET, HTMS-PET, PLL-PET, APTES-PET, and PEI(b)-PET, respectively. These various functional groups formed strong hydrogen bonds with PET hydroxyl groups. To analyze the surface potential of the surface functionalized PETs, the functionalized PETs were measured by KPFM. The surface potential results of the halogen-terminated surface functionalization PET had a similar tendency as the electron affinity of the halogen atoms, Cl > F > Br [**72**]. However, the aminated surface functionalization PETs did not have a clear tendency of the atoms, but the PEI(*b*)-PET had the most positive charge due to the branched structure of the PEI(*b*). Using positively modified PETs and negatively modified PETs, they fabricated 20 pairs of different TENGs. **Fig. 9b.** demonstrated the output power density by examining 20 pairs of different TENG results. All vertical contact and separation mode TENGs were tested under the 0.15 MPa at 2 Hz. The Cl-PET and PEI(*b*)-PET pair TENG achieved a maximum power density of approximately 55 W m^{-2}, which was 2 order higher values of the HPET and PEI(1) pair TENG. Thus, a simple surface functionalization strategy provides a wide range of triboelectric polymer properties and enhances the power performance.

The other approach is the reliable ion doping effect on the triboelectric property of the polymer contact layers to achieve high-performance TENGs. *Ryu et al* reported that polymer friction layers of TENG could enhance the triboelectric properties by adding electrolytes with asymmetric ion pairing [**73**]. **Fig. 10a.** showed schematic images of the polyvinyl alcohol

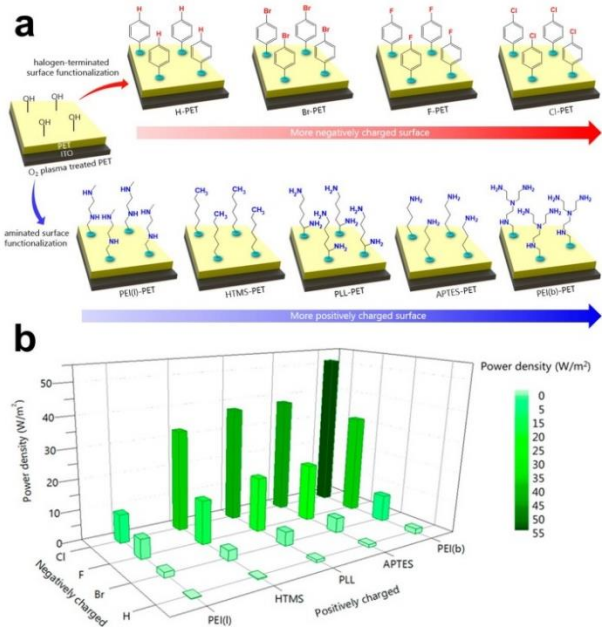

Fig. 9. (a) Schematic representations of functionalized PETs with adopted molecules. (b) Power density plot of 20 different contact pair TENGs. Adapted from Ref. [**70**] with permission from American Chemical Society.

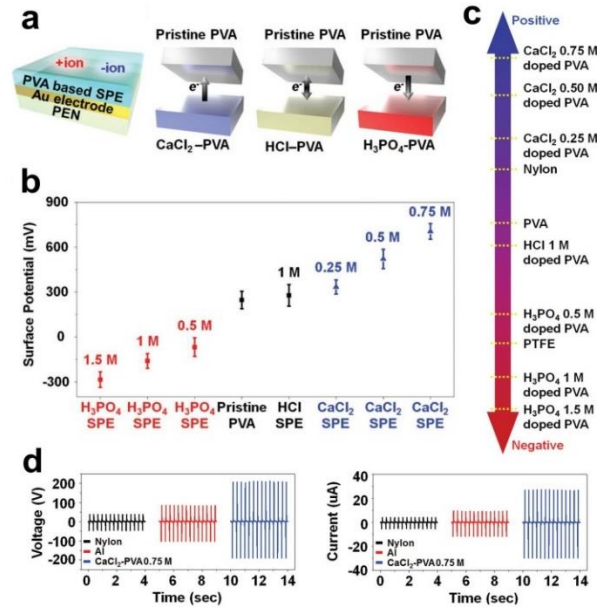

Fig. 10. (a) Schematic description of the SPE-TENGs. (b) KPFM surface potential results of SPEs. (c) Modified triboelectric series of SPEs. (d) Output voltage and current for TENGs with different triboelectric layers. Adapted from Ref. [**73**] with permission from Wiley.

(PVA) based solid polymer electrolyte (SPE) TENG and described the possible triboelectric properties of the SPEs after contact with the PVA, such as more positive, more negative or the same triboelectric property than PVA. Surface potentials of $CaCl_2$, H_3PO_4 and HCl SPEs were analyzed to study the ion pair effect on the triboelectric property of polymers using KPFM. 0.25 M to 0.75 M $CaCl_2$-PVA based SPEs, 0.5 to 1.5 M H_3PO_4-PVA based SPEs and 1M HCl-PVA based SPE was examined. In **Fig. 10b.**, the concentration of the

electrolyte and type of ions significantly changed the surface potential of the PVA-based SPEs. The surface potential of H_3PO_4-PVA SPE, which had more cations than anions, changed from +247 to −285 mV, and the result of H_3PO_4-PVA SPE showed more negative triboelectric property than pristine PVA. In contrast, the surface potential of $CaCl_2$-PVA SPE, which had more anions than cations, changes from +247 to +705 mV, and the result of $CaCl_2$-PVA SPE showed more positive triboelectric properties than pristine PVA. However, the surface potential of HCl-PVA SPE, which had equal anions and cations, did not change, and the result of HCl-PVA SPE showed similar triboelectric properties like pristine PVA. Based on these results, they modified the triboelectric series of the SPEs, PTFE, nylon and PVA (see **Fig. 10c.**). To compare the output performance of the nylon-PTFE, Al-PTFE and SPE-PTFE pair TENGs, they fabricated 16 cm^2 square TENGs. The output performance of the nylon-PTFE pair TENG and Al-PTFE pair TENG were 86 V and 8.7 μA, and 40 V and 4 μA, respectively, because Al had sufficient free electrons and could generate more surface triboelectric charges than nylon during the contact process. Significantly, the $CaCl_2$-PVA 0.75 M SPE-PTFE pair TENG was generated over 211 V and 27 μA and it offered much higher power performance than the Al-PTFE pair TENG. Therefore, the ion-doping strategy provides a wide modifying range of triboelectric polymer properties and enhances the power performance.

Conclusion and future perspectives

Over the last few years, autonomous smart sensors and network systems have been developed to realize a smart network society. In particular, the importance of user-friendly smart electronic devices, including multifunction, portable and permanent operation, will be needed in the near future. In addition, independent energy sources are highly desirable. Although smart electronic devices have been developed to be smaller and smarter, its power sources are still limited. Thus, despite developing smart systems to reduce power consumption, limited power sources offer limited operating time. As a result, it is necessary to extend the operating time. Therefore, the demand for self-driven sensors and systems is increasing to overcome this time-limited system. Among energy-harvesting systems, TENG is a feasible energy generator that uses widespread, abundant mechanical energy in our daily life. When two dissimilar materials are in contact with each other, the interface between the two materials generates surface charges with opposite polarity, which are known as triboelectric charges. Therefore, the triboelectric polymer layers determine the power performance and efficiency of the TENG. In this paper, the power performance and development of the triboelectric polymer is analyzed using the vertical contact and separation mode TENG. In terms of enhancing the output performance, material research and development has made significant progress based on the *V-Q-x* relationship. We discussed various approaches to increase the triboelectric surface charge density, the importance of proper balance between ample spacing and contact point density, and overcoming the typical limitations of TENG. Moreover, polymer development can be further used to enhance and control the triboelectric properties. To improve the TENG performance via miniaturization and high power density, new effective triboelectric materials have been developed. In particular, the discovery of new materials and the development of conventional material strategies will lead to dramatic synergies. Therefore, continuous effort to develop TENGs is instrumental to realize self-powered permanent IoT systems in the future.

Acknowledgements

This work was financially supported by the Industrial Strategic Technology Development Program (10052668, Development of wearable self-powered energy source and low-power wireless communication system for a pacemaker) and "Human Resources Program in Energy Technology" of the Korea Institute of Energy Technology Evaluation and Planning (KETEP, No. 20154030200870), granted financial resource from the Ministry of Trade, Industry & Energy, Republic of Korea.

References

1. Gubbi, J.; Buyya, R.; Marusic, S.; Palaniswami, M.; *Future Gener. Comput. Syst.*, **2013**, *29*, 1645. **DOI:** 10.1016/j.future.2013.01.010
2. Atzori, L.; Iera, A.; Morabito, G.; *Computer Networks*, **2010**, *54*, 2787. **DOI:** 10.1016/j.comnet.2010.05.010
3. Ning, H.;Liu, H.; *Adv. Internet Things*, **2012**, *02*, 1. **DOI:** 10.4236/ait.2012.21001
4. Guo, B.; Zhang, D.; Wang, Z.; Yu, Z.; Zhou, X.; *J. Netw. Comput. Appl.*, **2013**, *36*, 1531. **DOI:** 10.1016/j.jnca.2012.12.028
5. Stankovic, J. A.; *IEEE Internet Thing. J.*, **2014**, *1*, 3. **DOI:** 10.1109/jiot.2014.2312291
6. Mukhopadhyay, S. C.; Suryadevara, N. K.; Internet of things: challenges and opportunities; Springer: German, **2014**. **DOI:** 10.1007/978-3-319-04223-7_1
7. Al-Fuqaha, A.; Guizani, M.; Mohammadi, M.; Aledhari, M.; Ayyash, M.; *IEEE Commun. Surv. Tut.*, **2015**, *17*, 2347. **DOI:** 10.1109/comst.2015.2444095
8. Sundmaeker, H.; Guillemin, P.; Friess, P.; Woelfflé, S.; Vision and challenges for realizing the internet of things; European Commision: Luxembourg, **2010.** **DOI:** 10.2759/26127
9. Wang, Z. L.; *ACS Nano*, **2013**, *7*, 9533. **DOI:** 10.1021/nn404614z
10. Hwang, B.-U.; Lee, J.-H., Trung, T. Q.; Roh, E.; Kim, D.-I.; Kim, S.-W.; Lee, N.-E.; *ACS Nano*, **2015**, *9*, 8801 **DOI:** 10.1021/acsnano.5b01835
11. Wang, Z. L.; Song, J.; *Science*, **2006**, *312*, 242. **DOI:** 10.1126/science.1124005
12. Wang, X.; Song, J.; Liu, J.; Wang, Z. L.; *Science*, **2007**, *316*, 102. **DOI:** 10.1126/science.1139366
13. Qin, Y.; Wang, X.; Wang, Z. L.; *Nature*, **2008**, *451*, 809. **DOI:** 10.1038/nature06601
14. Mitcheson, P. D.; Yeatman, E. M.; Rao, G. K.; Holmes, A. S.; Green, T. C.; *Proc. IEEE*, **2008**, *96*, 1457. **DOI:** 10.1109/jproc.2008.927494
15. O'Regan, B.; Graetzel, M.; *Nature*, **1991**, *353*, 737. **DOI:** 10.1038/353737a0
16. Venkatasubramanian, R.; Siivola, E.; Colpitts, T.; O'quinn, B.; *Nature*, **2001**, *413*, 597. **DOI:** 10.1038/35098012

17. Shin, K. S.; Kim, T. Y.; Yoon, G. C.; Gupta, M. K.; Kim, S. K.; Seung, W.; Kim, H.; Kim, S.; Kim, S.; Kim, S. W.; *Adv. Mater.*, **2014**, *26*, 5619. **DOI:** 10.1002/adma.201400405
18. Lee, K. H.; Kim, T. H.; Shin, H. J.; Kim, S. W.; *Adv. Mater.*, **2016**, *28*, 1793. **DOI:** 10.1002/adma.201504865
19. Harman, T. C.; Taylor, P. J.; Walsh, M. P.; LaForge, B. E.; *Science*, **2002**, *297*, 2229. **DOI:** 10.1126/science.1072886S
20. Hochbaum, A. I.; Chen, R.; Delgado, R. D.; Liang, W.; Garnett, E. C.; Najarian, M.; Majumdar, A.; Yang, P.; *Nature*, **2008**, *451*, 163. **DOI:** 10.1038/nature06381
21. Lee, J.-H.; Ryu, H.; Kim, T.-Y.; Kwak, S.-S.; Yoon, H.-J.; Kim, T.-H.; Seung, W.; Kim, S.-W.; *Adv. Energy Mater.*, **2015**, *5*, 1500704. **DOI:** 10.1002/aenm.201500704
22. Lee, J. H.; Lee, K. Y.; Gupta, M. K.; Kim, T. Y.; Lee, D. Y.; Oh, J.; Ryu, C.; Yoo, W. J.; Kang, C. Y.; Yoon, S. J.; Yoo, J. B.; Kim, S. W.; *Adv. Mater.*, **2014**, *26*, 765. **DOI:** 10.1002/adma.201303570
23. Lee, J.-H.; Yoon, H.-J.; Kim, T. Y.; Gupta, M. K.; Lee, J. H.; Seung, W.; Ryu, H.; Kim, S.-W.; *Adv. Funct. Mater.*, **2015**, *25*, 3203. **DOI:** 10.1002/adfm.201500856
24. Lee, K. Y.; Kim, D.; Lee, J.-H.; Kim, T. Y.; Gupta, M. K.; Kim, S.-W.; *Adv. Funct. Mater.*, **2014**, *24*, 37. **DOI:** 10.1002/adfm.201301379
25. Lee, J. H.; Hinchet, R.; Kim, T. Y.; Ryu, H.; Seung, W.; Yoon, H. J.; Kim, S. W.; *Adv. Mater.*, **2015**, *27*, 5553. **DOI:** 10.1002/adma.201502463
26. Khan, U.; Kim, T.-H.; Lee, K. H.; Lee, J.-H.; Yoon, H.-J.; Bhatia, R.; Sameera, I.; Seung, W.; Ryu, H.; Falconi, C.; Kim, S.-W.; *Nano Energy*, **2015**, *17*, 356. **DOI:** 10.1016/j.nanoen.2015.09.007
27. Lee, K. Y.; Gupta, M. K.; Kim, S.-W.; *Nano Energy*, **2015**, *14*, 139. **DOI:** 10.1016/j.nanoen.2014.11.009
28. Seung, W.; Yoon, H.-J.; Kim, T. Y.; Ryu, H.; Kim, J.; Lee, J.-H.; Lee, J. H.; Kim, S.; Park, Y. K.; Park, Y. J.; Kim, S.-W.; *Adv. Energy Mater.*, **2017**, *7*, 1600988. **DOI:** 10.1002/aenm.201600988
29. Jing, Q.; Zhu, G.; Wu, W.; Bai, P.; Xie, Y.; Han, R. P. S.; Wang, Z. L.; *Nano Energy*, **2014**, *10*, 305. **DOI:** 10.1016/j.nanoen.2014.09.018
30. Su, Y.; Yang, Y.; Zhong, X.; Zhang, H.; Wu, Z.; Jiang, Y.; Wang, Z. L.; *ACS Appl. Mater. Interfaces*, **2014**, *6*, 553. **DOI:** 10.1021/am404611h
31. Zhu, G.; Chen, J.; Zhang, T.; Jing, Q.; Wang, Z. L.; *Nat. Commun.*, **2014**, *5*, 3426. **DOI:** 10.1038/ncomms4426
32. Lee, J.-H.; Kim, J.; Kim, T. Y.; Al Hossain, M. S.; Kim, S.-W.; Kim, J. H.; *J. Mater. Chem. A*, **2016**, *4*, 7983. **DOI:** 10.1039/c6ta01229a
33. Wang, Z. L.; Wu, W.; *Angew. Chem. Int. Ed. Engl.*, **2012**, *51*, 11700. **DOI:** 10.1002/anie.201201656
34. Khan, U.; Hinchet, R.; Ryu, H.; Kim, S.-W.; *APL Mater.*, **2017**, *5*, 073803. **DOI:** 10.1063/1.4979954
35. Cui, S.; Goldsmith, A. J.; Bahai, A.; *IEEE J. Sel. Area Commun.*, **2004**, *22*, 1089. **DOI:** 10.1109/jsac.2004.830916
36. Lee, K. Y.; Yoon, H.-J.; Jiang, T.; Wen, X.; Seung, W.; Kim, S.-W.; Wang, Z. L.; *Adv. Energy Mater.*, **2016**, *6*, 1502566. **DOI:** 10.1002/aenm.201502566
37. Chun, J.; Ye, B. U.; Lee, J. W.; Choi, D.; Kang, C. Y.; Kim, S. W.; Wang, Z. L.; Baik, J. M.; *Nat. Commun.*, **2016**, *7*, 12985. **DOI:** 10.1038/ncomms12985
38. Zi, Y.; Wang, J.; Wang, S.; Li, S.; Wen, Z.; Guo, H.; Wang, Z. L.; *Nat. Commun.*, **2016**, *7*, 10987. **DOI:** 10.1038/ncomms10987
39. Chan, C. K.; Peng, H.; Liu, G.; Mcilwrath, K.; Zhang, X. F.; Huggins, R. A.; Cui, Y.; *Nat. Nanotechnol.*, **2008**, *3*, 31. **DOI:** 10.1038/nnano.2007.411
40. Khan, U.; Kim, T. H.; Ryu, H.; Seung, W.; Kim, S. W.; *Adv. Mater.*, **2017**, *29*, **DOI:** 10.1002/adma.201603544
41. Kim, H.-J.; Kim, J.-H.; Jun, K.-W.; Kim, J.-H.; Seung, W.-C.; Kwon, O. H.; Park, J.-Y.; Kim, S.-W.; Oh, I.-K.; *Adv. Energy Mater.*, **2016**, *6*, 1502329. **DOI:** 10.1002/aenm.201502329
42. Kwak, S. S.; Lin, S.; Lee, J. H.; Ryu, H.; Kim, T. Y.; Zhong, H.; Chen, H.; Kim, S. W.; *ACS Nano*, **2016**, *10*, 7297. **DOI:** 10.1021/acsnano.6b03032
43. Choi, H.-J.; Lee, J. H.; Jun, J.; Kim, T. Y.; Kim, S.-W.; Lee, H.; *Nano Energy*, **2016**, *27*, 595. **DOI:** 10.1016/j.nanoen.2016.08.014
44. Kim, S.; Gupta, M. K.; Lee, K. Y.; Sohn, A.; Kim, T. Y.; Shin, K. S.; Kim, D.; Kim, S. K.; Lee, K. H.; Shin, H. J.; Kim, D. W.; Kim, S. W.; *Adv. Mater.*, **2014**, *26*, 3918. **DOI:** 10.1002/adma.201400172
45. Wang, J.; Li, S.; Yi, F.; Zi, Y.; Lin, J.; Wang, X.; Xu, Y.; Wang, Z. L.; *Nat. Commun.*, **2016**, *7*, 12744. **DOI:** 10.1038/ncomms12744
46. Pang, Y. K.; Li, X. H.; Chen, M. X.; Han, C. B.; Zhang, C.; Wang, Z. L.; *ACS Appl. Mater. Interfaces*, **2015**, *7*, 19076. **DOI:** 10.1021/acsami.5b04516
47. Pu, X.; Liu, M.; Li, L.; Zhang, C.; Pang, Y.; Jiang, C.; Shao, L.; Hu, W.; Wang, Z. L.; *Adv. Sci.*, **2016**, *3*, 1500255. **DOI:** 10.1002/advs.201500255
48. Zheng, Q.; Shi, B.; Li, Z.; Wang, Z. L.; *Adv. Sci.*, **2017**, 1700029. **DOI:** 10.1002/advs.201700029
49. Lee, J.W.; Cho, H. J.; Chun, J.; Kim, K. N.; Kim, S.; Ahn, C. W.; Kim, I. W.; Kim, J.-Y.; Kim, S.-W.; Yang, C.; Baik, J. M.; *Sci. Adv.*, **2017**, *3*, e1602902. **DOI:** 10.1126/sciadv.1602902S
50. Quan, Z.; Han, C. B.; Jiang, T.; Wang, Z. L.; *Adv. Energy Mater.*, **2016**, *6*, 1501799. **DOI:** 10.1002/aenm.201501799
51. Kang, H.; Kim, H.; Kim, S.; Shin, H. J.; Cheon, S.; Huh, J.-H.; Lee, D. Y.; Lee, S.; Kim, S.-W.; Cho, J. H.; *Adv. Funct. Mater.*, **2016**, *26*, 7717. **DOI:** 10.1002/adfm.201603199
52. Han, S. A.; Lee, K. H.; Kim, T.-H.; Seung, W.; Lee, S. K.; Choi, S.; Kumar, B.; Bhatia, R.; Shin, H.-J.; Lee, W.-J.; Kim, S.; Kim, H. S.; Choi, J.-Y.; Kim, S.-W.; *Nano Energy*, **2015**, *12*, 556. **DOI:** 10.1016/j.nanoen.2015.01.030
53. Hinchet, R.; Seung, W.; Kim, S.-W.; *ChemSusChem*, **2015**, *8*, 2327. **DOI:** 10.1002/cssc.201403481
54. Niu, S.; Wang, S.; Lin, L.; Liu, Y.; Zhou, Y. S.; Hu, Y.; Wang, Z. L.; *Energy Environ. Sci.*, **2013**, *6*, 3576. **DOI:** 10.1039/c3ee42571a
55. Saurenbach, F.; Wollmann, D.; Terris, B. D.; Diaz, A. F.; *Langmuir*, **1992**, *8*, 1199. **DOI:** 10.1021/la00040a030
56. Park, C. H.; Park, J. K.; Jeon, H. S.; Chun, B. C.; *J. Electrostat.*, **2008**, *66*, 578. **DOI:** 10.1016/j.elstat.2008.07.001
57. Cao, X.; Jie, Y.; Wang, N.; Wang, Z. L.; *Adv. Energy Mater.*, **2016**, *6*, 1600665. **DOI:** 10.1002/aenm.201600665
58. Zhang, L.; Yu, Y.; Eyer, G. P.; Suo, G.; Kozik, L. A.; Fairbanks, M.; Wang, X.; Andrew, T. L.; *Adv. Mater. Technol.*, **2016**, *1*, 1600147. **DOI:** 10.1002/admt.201600147
59. Wang, J.; Wen, Z.; Zi, Y.; Zhou, P.; Lin, J.; Guo, H.; Xu, Y.; Wang, Z. L.; *Adv. Funct. Mater.*, **2016**, *26*, 1070. **DOI:** 10.1002/adfm.201504675
60. Zi, Y.; Niu, S.; Wang, J.; Wen, Z.; Tang, W.; Wang, Z. L.; *Nat. Commun.*, **2015**, *6*, 8376. **DOI:** 10.1038/ncomms9376

61. Tang, W.; Jiang, T.; Fan, F. R.; Yu, A. F.; Zhang, C.; Cao, X.; Wang, Z. L.; *Adv. Funct. Mater.*, **2015**, *25*, 3718. **DOI:** 10.1002/adfm.201501331
62. Lee, J. H.; Hinchet, R.; Kim, S. K.; Kim, S.; Kim, S.-W.; *Energy Environ. Sci.*, **2015**, *8*, 3605. **DOI:** 10.1039/c5ee02711j
63. Paul, D. R.; Robeson, L. M.; *Polymer*, **2008**, *49*, 3187. **DOI:** 10.1016/j.polymer.2008.04.017
64. Kim, J.; Lee, J. H.; Ryu, H.; Lee, J.-H.; Khan, U.; Kim, H.; Kwak, S. S.; Kim, S.-W.; *Adv. Funct. Mater.*, **2017**, *27*, 1700702. **DOI:** 10.1002/adfm.201700702
65. Knotts, G.; Bhaumik, A.; Ghosh, K.; Guha, S.; *Appl. Phys. Lett.*, **2014**, *104*, 233301. **DOI:** 10.1063/1.4880119
66. Ma, W.; Zhang, J.; Chen, S.; Wang, X.; *J. Macromol. Sci. B*, **2008**, *47*, 434. **DOI:** 10.1080/00222340801954811
67. Indolia, A. P.; Gaur, M. S.; *J. Therm. Anal. Calorim.*, **2012**, *113*, 821. **DOI:** 10.1007/s10973-012-2834-0
68. Ma, W.; Zhang, J.; Wang, X.; Wang, S.; *Appl. Surf. Sci.*, **2007**, *253*, 8377. **DOI:** 10.1016/j.apsusc.2007.04.001
69. Lonjon, A.; Laffont, L.; Demont, P.; Dantras, E.; Lacabanne, C.; *J. Phys. D Appl. Phys.*, **2010**, *43*, 345401. **DOI:** 10.1088/0022-3727/43/34/345401
70. Shin, S. H.; Bae, Y. E.; Moon, H. K.; Kim, J.; Choi, S. H.; Kim, Y.; Yoon, H. J.; Lee, M. H.; Nah, J.; *ACS Nano*, **2017**, *11*, 6131. **DOI:** 10.1021/acsnano.7b02156
71. Wolf, R.; Sparavigna, A. C.; *Engineering*, **2010**, *02*, 397. **DOI:** 10.4236/eng.2010.26052
72. Rienstra-Kiracofe, J. C.; Tschumper, G. S.; Schaefer III , H. F.; *Chem. Rev.*, **2002**, *102*, 231. **DOI:** 10.1021/cr990044u
73. Ryu, H.; Lee, J.-H.; Kim, T.-Y.; Khan, U.; Lee, J. H.; Kwak, S. S.; Yoon, H.-J.; Kim, S.-W.; *Adv. Energy Mater.*, **2017**, 1700289. **DOI:** 10.10.2017002802/ae

